GLOBAL GYROKINETIC SIMULATIONS OF ISOTOPE EFFECTS FOR FUTURE TOKAMAK PLASMA CORE AND PEDESTAL

Lei Qi
Korea Institute of Fusion Energy
Daejeon, South Korea
Email: qileister@kfe.re.kr

T. S. Hahm
Seoul National University
Seoul, South Korea

Jae-Min Kwon, M. Leconte, M. J. Choi
Korea Institute of Fusion Energy
Daejeon, South Korea

Abstract

Isotope effects in both tokamak plasma core and pedestal regions from past (current) to future takamas are investigated utilizing the first principle global δf electrostatic gyrokinetic simulations. In the core region, we report a reversal in the isotopic dependence of energy confinement with increasing system size ρ^{*-1}. The favorable isotope effects on the energy confinement observed in past and present-day tokamaks may diminish or reverse in future tokamaks with significantly larger ρ^{*-1}. This finding offers critical insights for the design of future tokamaks, such as ITER, DEMO and fusion plants, particularly those with larger sizes or stronger magnetic fields. The primary mechanism driving this reversal is the isotope mass dependence of the turbulence radial correlation length, which is significantly weaker than Bohm scaling at low ρ^{*-1} and closer to gyro-Bohm scaling at high ρ^{*-1}. In the pedestal region, we confirm favorable isotope effects on energy confinement, consistent with experimental findings that show reduced L-H transition power thresholds for heavier isotopes. Large-scale, non-local, and non-diffusive avalanche transport is observed to dominate in the pedestal scenarios. Role of avalanches in isotope effects, as well as the interactive effects with equilibrium mean flows is currently under investigation in the pedestal region, and will be reported later.

1. INTRODUCTION

Hydrogen isotopes, deuterium (D) and tritium (T) are the most favorable candidates as the fusion reaction fuels to achieve controlled fusion energy. DT fusion possesses the lagest fusion cross section comparing to other reactions, such as DD, D^3He and $p^{11}B$ etc.. One of crucial objectives of ITER is the reactor-level operation with D and T. Therefore, understanding the role of isotopes has been a long-standing critical topic in fusion research.

Tokamak experiments involving tritium are rare, dating back 30 years to 1990s with the TFTR[1] and JET with a carbon wall[2]. Recently, significant efforts have been dedicated to experiments on JET with an ITER-like wall involving tritium[3]. Experiments on past and present-day tokamaks have demonstrated a favorable isotopic dependence of the energy confinement across different operational regimes, yielding an empirical scaling $\tau_E \propto M_i^\sigma$. The exponent σ is positive; τ_E represents the energy confinement time, and M_i denotes the isotope mass ratio to hydrogen. Empirical scaling laws, such as L-mode confinement scaling ITER89-P[4] and the H-mode confinement scaling ITER-IPB(y)[5], indicate $\sigma = 0.5$ and 0.2, respectively. With ITPA activities, a recent update of H-mode data from JET-ILW and ASDEX-Upgrade (AUG) indicates the exponent σ to be in the range of 0.09-0.47[6]. The favorable isotopic dependence of energy confinement has also been observed in an alternative magnetic configuration, stellarators[7,8,9].

The high-confinement mode (H-mode) characterized by a steep edge transport barrier is a promising operational regime for future coming tokamaks, such as ITER, DEMO and fusion plants, which aim to operate or pruduce fusion energy with deuterium-tritium (D-T). Understanding isotope effects in H-mode plasmas, especially the pedestal region is therefore a critical issue in magnetically confined fusion plasmas. For decades, world-wide researchers have spent substantial efforts investigating this issue and made great progress in many aspects, such as the isotopic dependence of global energy confinement in H-mode plasmas, L-H transition threshold and pedestal structures, etc. utilizing multi-devices across the world[10].

Isotopes have been found to enhance the global energy confinement in H-mode plasmas, as concluded in the empirical scaling law, e.g. IPB98(y,2) by ITER Physics Expert Group[5], which indicates the global energy confinement time $\tau_E \propto M_i^{0.19}$ in ELMy H-mode plasmas. Recently, an updated ITPA global H-mode energy

confinement scaling ITPA20 yields a similar isotopic dependence, $\tau_E \propto M_i^{0.20}$ in ELMy H-mode plasmas[6]. In H-mode, though the core plasma contains the most absorbed energy, pedestal with a sharp transport barrier contributes significantly to the overall confinement. Understanding the isotopic dependence of energy confinement in the pedestal is critical for investigating the global confinement in H-mode. Direct study of isotope effects in pedestal energy confinement is rare. Alternatively, great efforts have been devoted to unravelling the role of isotopes in the L-H transition threshold (P_{L-H}) and pedestal structures, such as width, height etc.. P_{L-H} indicates the minimum power input to triger a transition from L-mode to H-mode. Pedestal height can be an important factor incluences the pressure level in plasma core. It has been widely observed that isotopes can significantly reduce the L-H transition threshold $P_{L-H} \propto M_i^{-1}$[11-14], indicating a better pedestal energy confinement with higher ion mass.

Predictions for future tokamaks and fusion plants heavily rely on these existing results. However, extrapolations to future tokamaks and fusion plants based on these scaling laws may encounter unexpected changes in trend, induced by substantial dimensional disparities between current (and past) tokamaks and future ones with high magnetic field or large device sizes. There are evident system size gaps in the dimensionless parameter $\rho^{*-1} \equiv a/\rho_i$, which is typically on the order of $\rho^{*-1} \sim 10^3$ for future tokamaks and fusion plants, compared to $\rho^{*-1} \sim 10^2$ for past and present-day tokamaks, which is much smaller. Therefore, dedicated investigations into the isotopic dependence of energy confinement from current to future tokamaks are highly desirable.

The value of gyrokinetic simulation and modelling of tokamaks lies in providing insights for the development of future laboratory machines and reactors, such as ITER, DEMO and fusion plants. Precise predictions for future tokamaks can greatly aid in the design of reactors and their associated heating systems. Gyrokinetic simulations already indicate that in future, larger tokamaks, the anomalous transport level will follow a gyro-Bohm scaling, in contrast to a Bohm scaling observed in smaller tokamaks[15, 16]. A subsequent study[17] further elaborates this system size dependence is directly influenced by the size of strong turbulence region rather than the tokamak's minor radius. Meanwhile, a flux-driven full-f simulation[18] has not observed a transition to gyro-Bohm scaling from a system size scan due to prevalent large-scale non-local transport avalanches.

In the last IAEA-FEC conference hold in London in 2023, we reported a dedicated gyrokinetic simulation that has quantitatively reproduced the empirical scaling law for the isotopic dependence of energy confinement as derived from past and present-day tokamaks[19]. A novel mechanism has been identified, in which the turbulence radial correlation length, $l_{cr} \propto M_i^{0.11}$, significantly deviates from gyro-Bohm scaling. This deviation has been demonstrated to be crucial for understanding isotope effects, prompting further investigation into the properties of turbulence radial correlation and their impact on energy confinement from past and current to future tokamaks. The quantitative agreement between the gyrokinetic simulations and experimental results from previous and present-day tokamaks provides a solid basis for exploring isotope effects in forthcoming tokamaks. In this work, we investigate the isotope effects in both plasma core and H-mode pedestal regions, extending from past (current) tokamaks with relatively small system size (ρ^{*-1}) to the future next-generation tokamaks with much larger sizes or stronger magnetic fields.

2. ISOTOPE EFFECTS IN THE CORE: REVERSAL IN SYSTEM SIZE SCANS

In this section, we report a reversal in the isotopic dependence of energy confinement with increasing system size ρ^{*-1} from electrostatic global δf gyrokinetic simulations using parameters in the tokamak plasma core regions. The favorable isotope effects on the energy confinement observed in past and present-day tokamaks may diminish or reverse in future tokamaks with significantly larger ρ^{*-1}. This finding offers critical insights for the design of future tokamaks, such as ITER, DEMO and fusion plants, particularly those with larger sizes or stronger magnetic fields. The primary mechanism driving this reversal is the isotope mass dependence of the turbulence radial correlation length, which is significantly weaker than Bohm scaling at low ρ^{*-1} and closer to gyro-Bohm scaling at high ρ^{*-1}.

2.1. Simulation tool and setup

In this study, the electrostatic global δf gyrokinetic particle-in-cell code gKPSP[20-23] is employed to simulate the system size effects on the isotopic dependence of energy confinement in the electrostatic limit. We focus on the Ohmic, L-mode and the core of H-mode plasmas, from which we select representative parameters. Normalized ion and electron temperature gradients are $R/L_{Ti} = 4.5$ and $R/L_{Te} = 7.5$ respectively, while density gradients are $R/L_{ni} = R/L_{ne} = 2.5$, wherein $L_x = -(d\ln x/dr)^{-1}$ and $R = 1.86$m is the major radius. The equilibrium profiles are fixed in δf simulations. Ion and electron temperatures at the plasma center are $T_{i0} = 2.725$keV and $T_{e0} = 5.5$keV, respectively. The minor radius is $a = 0.67$m, and the safety factor profile is set by $q = 0.58 + 3.04\varepsilon + 8.5\varepsilon^2$. Both the Coulomb collision operator for ion-ion collision and the

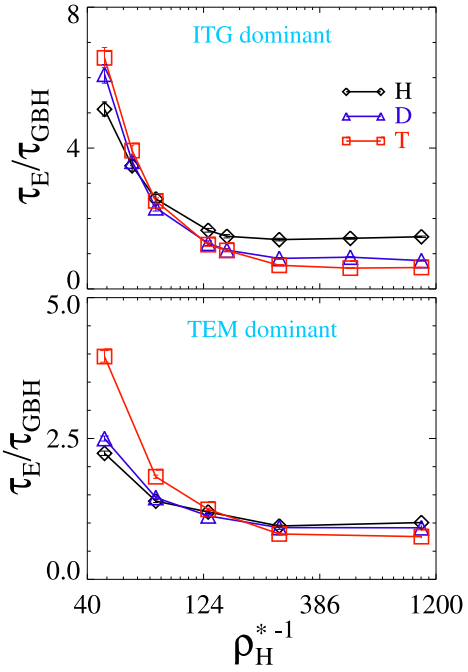

FIG. 1. System sizes ρ_H^{*-1} dependence of the normalized thermal energy confinement time τ_E/τ_{GBH} for hydrogen (H, black), deuterium (D, blue) and Tritium (T, red) in both ITG (top) and TEM (bottom) dominant turbulent transport. Statistical standard error bars are also added for all the data points. $x-$axis is in log scale.

Lorentz pitch-angle scattering operator for electron-ion collision are included in all simulations. Physics of zonal flow is also incorporated in nonlinear simulations self-consistently. Two densities, $n = 1.0 \times 10^{19} m^{-3}$ and $n = 8.0 \times 10^{19} m^{-3}$ are chosen to represent trapped electron mode (TEM) and ion temperature gradient mode (ITG) dominant cases, respectively. Radial profiles of temperature and density gradients are defined by the function $G(\varepsilon) = -\frac{R}{L_x} \exp\{-[(\varepsilon - \varepsilon_c)/\varepsilon_\Delta]^{20}\}$, where G represents the gradients, and ε is the inverse aspect ratio. $\varepsilon_c = 0.18$ and $\varepsilon_\Delta = 0.054$ determine the center and width of the finite gradient region respectively. With this configuration, using the finite gradient (turbulence unstable region) size, the dimensionless parameter ρ^* is redefined by $\rho_H^{*-1} \equiv 2\varepsilon_\Delta R/\rho_{iH}$ normalized to hydrogen mass. Here ρ_{iH} denotes the ion gyroradius for hydrogen, calculated as a radial average consistent with the analysis of transport and energy confinement time throughout the paper. This form of ρ_H^{*-1} reflects the physical source of system size effect, which is the result of the finite width of the unstable region in gyroradius units instead of the minor radius[17]. By varying the magnetic field, we scan the system sizes with ρ_H^{*-1} ranging from approximately 50 to over 10^3 for various isotopes' mass. For all cases with varying system sizes, the radial grid resolution is set to $\Delta r \simeq \rho_{iH}$, which has been verified through convergence tests to be sufficiently fine. In this setup, the radial grid number is adjusted according to the magnetic field but kept fixed across different isotopes. As a result, higher mass leads to finer radial resolution relative to the corresponding ρ_i, ensuring that all simulations remain within the converged regime. The poloidal wave number $k_\theta \rho_i \sim 1$ is ensured to cover both ITG and TEM turbulence regimes in all cases.

2.2. Observation of the reversal

To account for contributions from both electron and ion transport channels, we calculate the effective thermal energy transport diffusivity χ_{eff} according to Eq. 1, with $\chi_{e(i)}$ being electron (ion) heat transport diffusivity and $D_{e(i)}$ the electron (ion) particle flux diffusivity. Since these are global simulations, diffusivities are flux-surface and radially averaged in the turbulence domain. The energy confinement time can be calculated by $\tau_E = \Delta_{turb}^2/\chi_{eff}$, where $\Delta_{turb} = 2\epsilon_\Delta R$ is the size of turbulence unstable region. We introduce the normalization for the energy confinement $\tau_{GBH} = \Delta_{turb}^2/\chi_{GBH}$. Therefore, we have the normalized energy confinement time $\tau_E/\tau_{GBH} = \chi_{GBH}/\chi_{eff}$. Here $\chi_{GBH} = \rho_{iH}^2 V_{TiH}/a$ is the gyro-Bohm diffusivity for hydrogen mass. Figure 1 shows τ_E for varying system sizes ρ_H^{*-1}, isotopes, and for both ITG and TEM dominant turbulence. We note that ρ_H^{*-1} is the same for varying isotopes. Therefore, the isotope effects can be observed from the τ_E at the same ρ_H^{*-1}. A reversal in the isotopic dependence of energy confinement time is observed as ρ_H^{*-1} increases. Initially, isotopes enhance τ_E, which is favorable for energy confinement in smaller system sizes. However, as the system size increases, this trend reverses, and isotopes begin to reduce τ_E, which is unfavorable for energy confinement

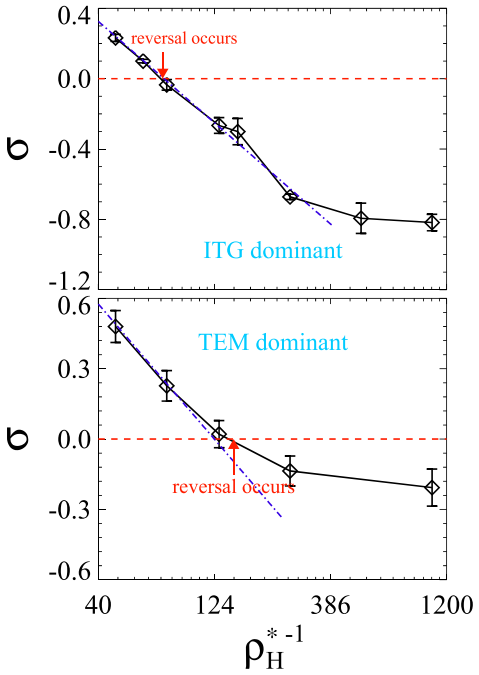

FIG. 2. Exponent σ is plotted with varying ρ_H^{*-1} for both ITG (top) and TEM (bottom) turbulence. Standard error bars from the power law fit are added for all data points. Red arrows indicate the ρ_H^{*-1}, where σ crosses 0 and reverses its sign. Blue dash-dot lines are by the formula $\sigma = -1.17 \log_{10} \rho_H^{*-1} + const.$.

in larger system sizes. This reversal is evident in both ITG and TEM turbulent transport.

$$\chi_{eff} = \frac{\chi_e n_e \frac{\partial T_e}{\partial r} + \chi_i n_i \frac{\partial T_i}{\partial r} + D_e T_e \frac{\partial n_e}{\partial r} + D_i T_i \frac{\partial n_i}{\partial r}}{n_e \frac{\partial T_e}{\partial r} + n_i \frac{\partial T_i}{\partial r} + T_e \frac{\partial n_e}{\partial r} + T_i \frac{\partial n_i}{\partial r}} \tag{1}$$

We perform a fit of the exponent for the energy confinement time with three isotopes' mass at the same ρ_H^{*-1} by $\tau_E \propto M_i^{\sigma}$ to quantitatively evaluate the isotope effects. The exponent σ can be obtained for varying ρ_H^{*-1} in both ITG and TEM turbulence, as depicted in Fig. 2. The figure reveals that σ is positive at low ρ_H^{*-1} indicating beneficial effects on energy confinement. However, σ gradually becomes negative at high ρ_H^{*-1}, signifying adverse effects on energy confinement. As ρ_H^{*-1} increases further, σ tends to saturate, suggesting that the degradation effects of isotopes on energy confinement may not worsen for sufficiently large system sizes. This trend is observed in both ITG and TEM turbulence. The discovery that isotopes may degrade energy confinement in future tokamaks with larger dimensions or stronger magnetic fields is significantly different from extrapolations based on scaling laws from past and present-day tokamaks (e.g., ITER89-P, ITER-IPB(y), etc.). The findings from this study provide novel insights for the design of future tokamaks and heating systems aimed at achieving burning plasmas.

2.3. Key physical mechanisms underlying the reversal

The key physical mechanism underlying this reversal trend of isotope effects lies in the investigation of turbulence radial correlation, as an extension of Ref. [19] to larger system sizes for future tokamaks. The radial correlation length is calculated using an average method based on turbulence intensity: $l_{cr} = 2\pi/\overline{k_r}$, with $\overline{k_r} \equiv \sqrt{\sum_{k_r,k_\theta,k_\zeta} k_r^2 |\phi(k_r,k_\theta,k_\zeta)|^2 / \sum_{k_r,k_\theta,k_\zeta} |\phi(k_r,k_\theta,k_\zeta)|^2}$. Similar to the analysis performed on the energy confinement time, we determine the exponent Δ from the power law fit $l_{cr} \propto M_i^{\Delta}$ for the radial correlation length. The dependence of Δ on the system size ρ_H^{*-1} is displayed in the Figure 3 for both ITG and TEM regimes. The figure shows a transition of Δ from a rapidly increasing regime to saturation as ρ_H^{*-1} increases, which is in close relation with the trend of exponent σ.

The mass dependence of the turbulence radial correlation length is significantly weaker than the gyro-Bohm scaling at small system sizes, but closer to it at larger sizes. The gyro-Bohm scaling suggests that the radial correlation length follows $l_{cr} \propto M_i^{0.5}$. Specifically, for sufficiently small system sizes as shown in the figure, Δ is less than 0.25, indicating the mass dependence of l_{cr} is weaker than the Bohm scaling, which implies $l_{cr} \propto M_i^{0.25}$.

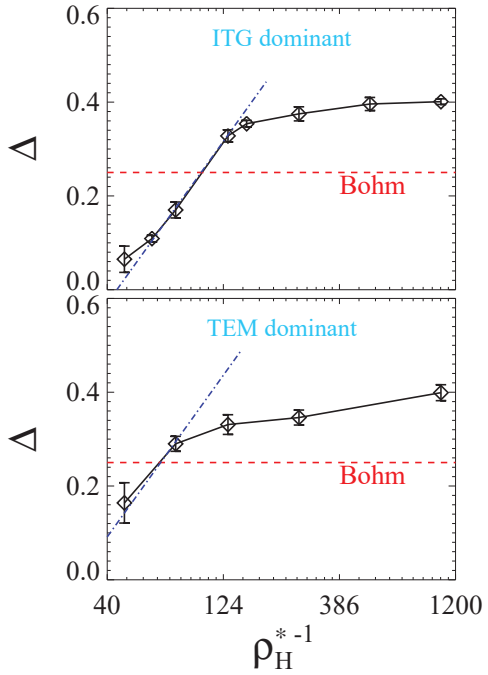

FIG. 3. Exponent Δ as a function of ρ_H^{*-1} for both ITG (top) and TEM (bottom) turbulence. Standard error bars from the power law fit are added for all data points. Blue dash-dot lines are by the formula $\Delta = 0.7 \log_{10} \rho_H^{*-1} + const.$. Red dash lines depict the Bohm scaling.

The system size dependence of the turbulence radial correlation length plays a crucial role in the reversal of the isotopic dependence of energy confinement from small to large system sizes. According to the dimensional analysis, the Bohm scaling implies no isotope effects from the relationships $\tau_E \propto 1/\chi \propto 1/l_{cr}^2\omega_c \propto M_i^0$. This further demonstrates that the behavior of the turbulence radial correlation length determines the transition of σ from a rapidly growing phase to saturation. Additionally, large-scale global transport phenomena-such as avalanching-can also break the gyroBohm scaling, as discussed in Ref.[18].

2.4. Summary and discussion

Gyrokinetic simulations with gKPSP reveal a reversal in the isotopic dependence of energy confinement as system sizes transition from small to large. This indicates that the beneficial effects of isotopes on energy confinement observed in current tokamaks might be diminished or even reversed in future tokamaks. The study shows that this reversal occurs with increasing ρ_H^{*-1}, offering valuable insights for the design of future tokamaks with larger sizes (e.g. ITER, DEMO and fusion plants) or stronger magnetic fields. Consequently, empirical scaling laws derived from present and past devices, like ITER89-P and ITER-IPB(y), may not be adequate for future tokamak designs. The primary mechanism behind this reversal is attributed to the isotope mass dependence of the turbulence radial correlation length, which is significantly weaker than Bohm scaling at low ρ_H^{*-1} and closer to gyro-Bohm scaling at high ρ_H^{*-1}. This finding differs from previous gyrokinetic simulations, which typically show only a direct transition from Bohm to gyro-Bohm scaling as the system size increases. It may offer new insights into the study of turbulence with limited spatial scales. In addition, our work also implies the study of impurity transport and energetic particle transport should consider the system size effects.

Experimental evidence already supports the trend of diminishing isotope effects with increasing tokamak device size, consistent with our predications for future large-scale tokamaks. For example, In section 3.2 of Ref. [5], it is reported that "The energy confinement time was found to be higher in deuterium plasmas relative to hydrogen ones, i.e., $\tau_E \propto A_i^\alpha$ with $\alpha = 0.5$ in small tokamaks and with $\alpha = 0.2$ in large machines such as JET and TFTR." More recent work also shows that isotope effects in global energy confinement in JET are relatively weak or even negligible[24]. Similar clues about the isotope effects' dependence on the device sizes for H-mode can also be drawn in Ref.[6]. These findings underscore the importance of systematically investigating the system size dependence of isotope effects. Cross-validation between numerical and experimental studies will be essential for improving our understanding and for extrapolating isotope behavior in future devices.

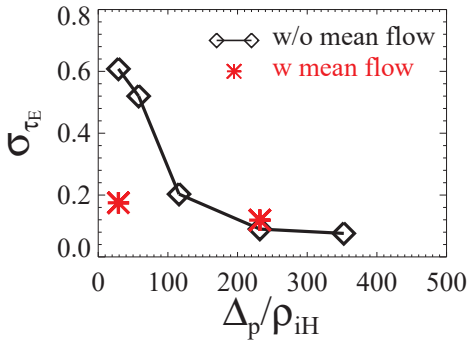

FIG. 4. The exponent σ_{τ_E} is plotted in terms of pedestal width Δ_p/ρ_{iH}. Black line and dimonds represent for scenarios without mean flow, and red asterisks indicate cases with mean flow.

3. ISOTOPE EFFECTS IN THE H-MODE PEDESTAL: ROLE OF AVALANCHES

In this section, we extend our study of isotope effects to the tokamak pedestal region.

3.1. simulation setup

Utilizing the global gyrokinetic simulation program gKPSP-which has been quantitatively validated against experimental scalings of isotopic dependence in the energy confinement time[19]-we extend our study to the H-mode pedestal and predict isotope effects for next-generation, larger tokamaks or machines with stronger magnetic fields. In our δf simulations, we fix the equilibrium profiles and adopt the following representative pedestal parameters: Normalized ion and electron temperature gradients are $R/L_{Ti} = R/L_{Te} = 80$, and density gradients are $R/L_{ni} = R/L_{ne} = 40$, wherein $L_x = -(d\ln x/dr)^{-1}$ and the major radius is $R = 1.86$m. At the pedestal top, ion and electron temperatures are $T_{i0} = T_{e0} = 1.0$keV, and the density is $n = 1.0 \times 10^{19} m^{-3}$. The minor radius is $a = 0.67$m, and the safety factor profile is $q(\varepsilon) = 0.58 + 34.0\varepsilon^2$. The pedestal region spans $r/a = 0.875$ to 0.90, giving $q = 4.13$ and magnetic shear $s_q = 1.72$ at its center. All simulations include the Coulomb collision operator for ion-ion collision and the Lorentz pitch-angle scattering operator for electron-ion collision. Nonlinear runs also self-consistently incorporate zonal flow physics. Radial profiles of temperature and density gradients are defined by the function $G(\varepsilon) = -\frac{R}{L_\varepsilon}\exp\{-[(\varepsilon-\varepsilon_c)/\varepsilon_\Delta]^4\}$, with ε the inverse aspect ratio, $\varepsilon_c = 0.32226$ and $\varepsilon_\Delta = 0.00895$. By varying the magnetic field from $5.25T$ to $63.0T$, we scan the pedestal width normalized by hydrogen gyroradius at the pedestal center Δ_p/ρ_{iH} from ~ 30 to ~ 400 for various isotopes' mass. Consequently, the temperature gradient scale length normalized by hydrogen gyroradius at the pedestal center L_T/ρ_{iH} spans roughly 40 to over 200. The poloidal wave number $k_\theta\rho_i \sim 1$ is ensured to cover both ITG and TEM turbulence regimes in all cases.

3.2. isotope effects on energy confinement in the pedestal

We compute the effective thermal energy transport diffusivity χ_{eff} according to Eq. 1. Given the global nature of our simulations, these diffusivities averaged over flux-surface and radially within the pedestal region. To facilitate comparison across different scenarios, χ_{eff} is normalized to the gyro-Bohm diffusivity for hydrogen mass at the pedestal center, defined as $\chi_{GBH} = \rho_{iH}^2 V_{TiH}/a$. Consequently, the thermal energy confinement time is calculated using $\tau_E \equiv a^2/\chi_{eff}$. We fit the energy confinement time to the scaling relation $\tau_E \propto M_i^{\sigma_{\tau_E}}$, where M_i is the ratio of isotope mass to hydrogen. The exponent σ_{τ_E}, as a function of Δ_p, is presented in the Figure 4. In this figure, the black line (dimonds) represents the analysis derived directly from Fig. **??** and scenarios without mean flow. The analysis indicates that $\sigma_{\tau_E} \simeq 0.6$ at small Δ_p and decreases Δ_p increases. This behavior suggests more favorable isotope effects on energy confinement at smaller pedestal width, aligning with observations in core scenarios where more favorable isotope effects are noted at lower system sizes[25]. However, unlike in the core cases, no reversal of the isotope effect is observed in this pedestal width scan. We note that this finding of favorable isotope effects on energy confinement in the pedestal also aligns with the experimental studies showing less L-H transition power threshold with higher ion mass. These difference between core and pedestal behaviors imply distinct underlying physical mechanisms, warranting further investigation in this study.

A pertinent and intriguing question arises: what accounts for the divergence in turbulence characteristics between the core and pedestal regions? This deviation suggests the presence of different underlying physical mechanisms governing turbulence and transport in the pedestal. One plausible explanation lies in the influence of

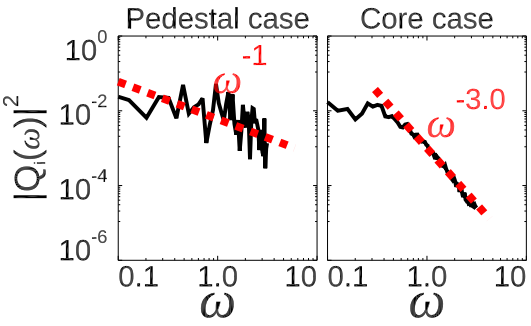

FIG. 5. Ion heat transport temporal Fourier spectra $|Q_i(\omega)|^2$ is presented as black lines for both pedestal (left) and core (right) cases.

large-scale global transport phenomena, such as transport avalanching[26-28]. The non-local and non-diffusive avalanching is intrinsic to the systems exhibiting self-similarity and a consequence of self-organized criticality (SOC), for instance the spectral power law scaling $S(f) \sim 1/f$. Here $S(f)$ is the spectral density with f being the frequency.

To investigate the hypothesis that avalanche-like transport phenomena contribute to the distinct turbulence behaviors observed between the pedestal and core regions, we compare the spectral properties of ion heat transport (Q_i) in both scenarios. Specifically, we analyze the $B_0 = 42$T pedestal case and the core case with $n = 8.0 \times 10^{19} m^{-3}$ and $B_0 = 42T$, as presented in Ref. [25]. Figure 5 displays the temporal Fourier spectra $|Q_i(\omega)|^2$ for both cases, where ω denotes the angular frequency. In the pedestal scenario, the spectrum follows a power-law scaling of $|Q_i(\omega)|^2 \propto \omega^{-1}$, indicative of self-organized criticality (SOC) associated with strong avalanche dynamics. Conversely, the core scenario exhibits a steeper scaling of $|Q_i(\omega)|^2 \propto \omega^{-3}$, suggesting the absence of significant avalanche transport.

3.3. Summary and discussion

We perform simulations in the tokamak pedestal region, characterized by steep pressure gradients near the edge, to investigate isotope effects. The simulations confirm the favorable isotope effect on energy confinement in the pedestal, consistent with experimental observations of a lower L-H transition power threshold for heavier isotopes. Prevalent large-scale, non-local, and non-diffusive transport avalanches are observed in the pedestal scenarios. Research work is ongoing to uncover the role of avalanches in isotope effects, as well as the interactive effects with equilibrium mean flows. It is important to note that while our study highlights the differing physics between core and pedestal regions, the fundamental distinction lies in the turbulence transport properties, particularly the presence of avalanche dynamics. In core cases exhibiting strong or weak avalanching, isotope effects may resemble those observed in pedestal scenarios—a hypothesis warranting further investigation.

ACKNOWLEDGEMENTS

This work is supported by the R&D Program through Korea Institute of Fusion Energy (KFE) funded by the Ministry of Science, ICT and Future Planning of the Republic of Korea (KFE-EN2441-10 and KFE-EN2541-11) and by the National R&D Program through the National Research Foundation of Korea (NRF) funded by the Korea government (Ministry of Science and ICT) (NRF-2021M1A7A4091135). Simulations were run on KFE KAIROS super computer.

REFERENCES

[1] S. D. Scott et al., Phys. Plasmas **2**, 2299-2307 (1995).

[2] J. Jacquinot (JET Team) et al., Nucl. Fusion **39**, 235 (1999).

[3] C. F. Maggi and JET contributors, Nucl. Fusion in progress (2024).

[4] P. N. Yushmanov et al., Nucl. Fusion **30**, 1999 (1990).

[5] ITER Physics Expert Group on Confinement and Transport et al., Nucl. Fusion **39**, 2175 (1999).

[6] G. Verdoolaege, et al., Nucl. Fusion **61**, 076006 (2021).

[7] H. Yamada, et al., Phys. Rev. Lett. **123**, 185001 (2019).

[8] K. Nagaoka, et al., Nucl. Fusion **59**, 106002 (2019).

[9] T. Kinoshita, et al., Phys. Rev. Lett. **123**, 235101 (2024).

[10] K. Ida, Rev. of Mod. Plasma Phys. **7**, 23 (2023).

[11] ASDEX Team, Nucl. Fusion **29**, 1959 (1989)

[12] C. F. Maggi et al., Plasma Phys. Control. Fusion **60**, 014045 (2018)

[13] L. M. Shao et al., Nucl. Fusion **61**, 016010 (2021)

[14] G. Birkenmeier et al., Nucl. Fusion **62**, 086005 (2022)

[15] Z. Lin, et al., Phys. Rev. Lett. **88**, 195004 (2002).

[16] Y. Xiao and Z. Lin, Phys. Rev. Lett. **103**, 085004 (2009).

[17] B. F. McMillan et al., Phys. Rev. Lett. **105**, 155001 (2010).

[18] Y. Idomura and M. Nakata, Phys. Plasmas **21**, 020706 (2014).

[19] L. Qi, et al., Phys. Rev. Research **6**, L012004 (2024).

[20] L. Qi, et al., Phys. Plasmas **23**, 062513 (2016).

[21] J. M. Kwon, et al., Comput. Phys. Commun. **215**, 81-90 (2017).

[22] L. Qi, Sci. Rept. **12**, 5042 (2022).

[23] Y. J. Kim, et al., Phys. Plasmas **29**, 042103 (2022).

[24] T. Tala et al., Nucl. Fusion **63**, 112012 (2023).

[25] Lei Qi et al., in submission (2025)

[26] Hahm T. S. and Diamond P. H., J. Korean Phys. Soc. **73**, 747-92 (2018).

[27] Garbet X., Laurent L., Samain, A. and Chinardet J., Nucl. Fusion **34**, 963-74 (1994).

[28] Diamond P. H. and Hahm T. S., Phys. Plasmas **2**, 3640-9 (1995).